Draft version November 8, 2024
Typeset using LaTeX default style in AASTeX631

Impacts of Ultraviolet Backgrounds on Circumgalactic Medium Ion Densities

Elias Taira,[1] Claire Kopenhafer,[1] and Brian W. O'Shea [2]

[1] *Michigan State University Department of Physics and Astronomy*
567 Wilson Rd, East Lansing
MI 48824

[2] *Department of Computational Mathematics, Science, and Engineering, Department of Physics and Astronomy, and Facility for Rare Isotope Beams, Michigan State University, East Lansing, MI 48824*

ABSTRACT

Amongst the many different features that go into simulations of the circumgalactic medium (CGM), the ultraviolet background (UVB), while playing a significant role in the ionization of different species within the CGM, is not fully understood. At this point in time, there are a variety of different models that have been created based on the quantity / intensity of different ultraviolet sources (i.e. stars and quasars). In this project, we perform pairwise comparisons of the ionization patterns of four different UVB models, specifically looking at how these models impact the ion column densities of individual gas clouds in the CGM. From our analysis we find evidence that shows UVB models produce significant changes in the ionization, but these differences are specific to the models' design and will require further investigation.

1. INTRODUCTION

Claire has written notes in this color :)
Brian's text is in this color. [BWO: Brian notes look like this]

The circumgalactic medium (CGM) is a multiphase medium that exists just outside of the disc of the galaxy and is typically observed via quasar absorption spectra. This method has been used in a number of observational surveys: COS-Halos (Tumlinson et al. (2013)), COS-Burst (Heckman et al. (2017)), COS CGM Compendium (Lehner et al. (2018)), KODIAQ and KODIAQ Z (Lehner et al. (2014); Lehner et al. (2016), Lehner et al. (2022)), Red Dead Redemption (Berg et al. (2019)), CASBaH (Burchett et al. (2018); Prochaska et al. (2019)), CUBS (Chen et al. (2020)), CGM2 (Wilde et al. (2021)). It is from these surveys that we have extracted a large amount of CGM metal ion absorber data from these spectra which can then be used to extract information about the physical properties of the CGM. However, there are several sources of uncertainty to consider when performing this analysis. Firstly, the chemical abundances of different ion species within the CGM. While solar abundance patterns are assumed by many studies (Hummels et al. (2013), Hummels, Smith, and Silvia (2017), Peeples et al. (2019), DeFelippis et al. (2021), and Butsky et al. (2022)), there is growing evidence indicating this may not be the case (Berg et al. 2019; Chen et al. 2020; Das et al. 2021; Gupta et al. 2021; Zahedy et al. 2021). Another source of uncertainty is the equilibrium ionization state of CGM species (Talk a bit about the history of UV background determination and the uncertainty around it.)

Additionally, to extract physical data from absorption spectra, the assumption is made that each absorption feature originates from a single gas cloud along the line of sight. This assumption is challenged in Marra et al. 2021 in which the authors perform a pilot study assessing how well standard absorption spectra processing techniques recover underlying gas properties (column density, temperature, metallicity, etc.) by analyzing synthetic COS & HIRES spectra of simulated galaxies. From this study, it was found that this assumption was only accurate in correctly predicting the average metallicity of the CGM. This methodology, in which its physical quantities are inferred based off the absorption spectra, is referred to as backwards modeling as we are moving backwards from observation to find the underlying physical phenomena. Conversely, forward modeling is the approach of starting from the physical phenomena, likely in a simulation, then letting the phenomena propagate into observation. While this method does have its own limitations, the information provided by working from the physical phenomena can prove vital to informing the inferences made by backward-modeling techniques.

To characterize these uncertainties, the goal of this work is to quantify the variation in absorber column density introduced by changing the UVB. We do this using the same set of cosmological simulations, post-processed by pipeline that is identical except for different choices of the UV background. We then compare those resulting column densities, gas densities and temperatures to identify notable features in the data. In section 2, we discuss our data selection, simulation pipeline, and general methodology for performing our analysis. In section 3, we present the results of our analysis, and in section 4, we interpret our findings and discuss the implications of our results in the broader research community. Finally, we summarize our findings and discuss possibilities for future research project in section 5.

2. METHODOLOGY

We organize our process in the form of a pipeline to help streamline our thought process, as highlighted in Fig. 1. We begin by obtaining our simulation data from the FOGGIE collaboration. Next, trident, a synthetic absorption spectra tool, is used to create rays throughout the FOGGIE galaxies. The trident data is then transferred through SALSA (Synthetic Absorption Line Surveyor Application) to obtain absorbers from each ray. For each set of SALSA absorbers created from each UVB, we generated a pairwise comparison to categorize each UVB into their different categories based on the spatial position of absorbers along the line of sight. Finally, we perform analysis on our results, evaluating their use in future observations of the CGM. In the following sections, we will go into more detail on each of the steps shown along the pipeline.

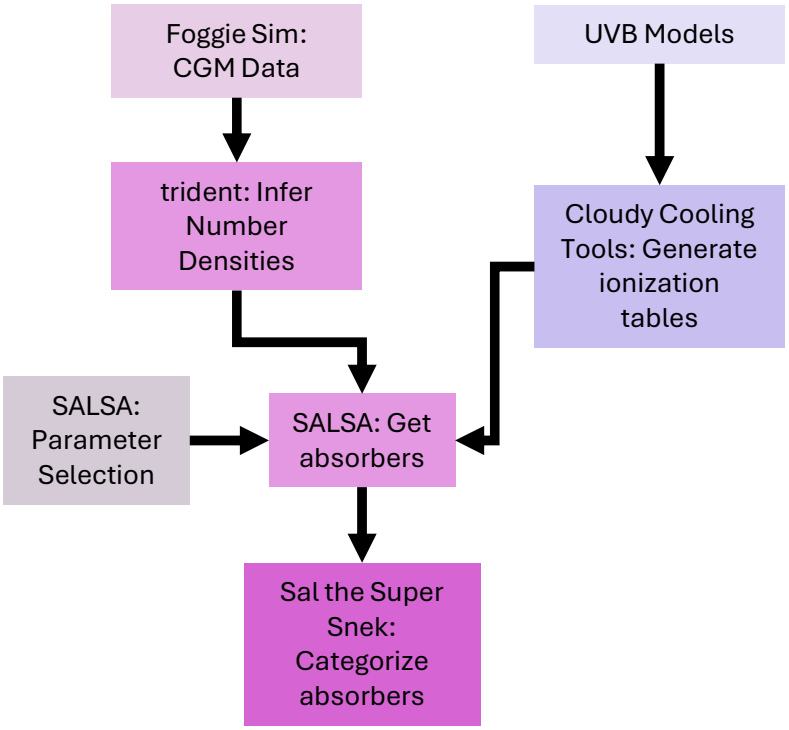

Figure 1: "Generate rays" means "infer ionic number densities given gas density, temperature, and HI density and metallicity." Obviously that won't fit in the flow chart but I would change the phrase "generate rays". Since you bothered to make separate colored blocks, the caption should relate color to subsection; e.g. light purple to Section 2.1 [BWO: I think that this figure is missing a box for Trident!]

2.1. *UVB*

For the UVB models we will be using, we have selected two different "families" of models for a total of four UVB models in total. These models include: Faucher-Giguere et al. from 2009 and 2020 (FG 2009 and FG 2020

respectively), and Puchwein et al. from 2019 (PCW 2019) and Haart & Madau 2012 (HM 2012). These models were selected specifically to allow us to analyze the differences between model families and compare the effectiveness of the model between generations. We'll need to summarize the updates that both of these models made; clearly something spurred the creation of new UVB models from both groups.

To include these UVB models in our analysis, we must first ensure that we have the models' ionization tables as referenced in Fig. 2. While the older generations of the Faucher-Giguere and Puchwein suites of models have these ionization tables generated, the younger generations of models have yet to be any readily available tables made for them. Thus, we rely on the Cloudy Cooling Tools software to generate these tables for both FG 2020 and PCW 2019. We use a series of one-zone CLOUDY models to determine the equilibrium ionization fractions for elements H I, C II, S III, Si IV, S IV, C IV, N V and O VI. We include self-shielding. Such ionization fraction tables have been made available for FG 2009 and HM 2012 thanks to Trident.

2.2. *Data Selection*

We base our analysis on the simulations run by the FOGGIE Collaboration, selecting galaxy 2392 (Hurricane) at redshifts ≈ 2.0-3.0, during cosmic noon when the intensity of UV radiation is very high due to the rapid formation of young stars.

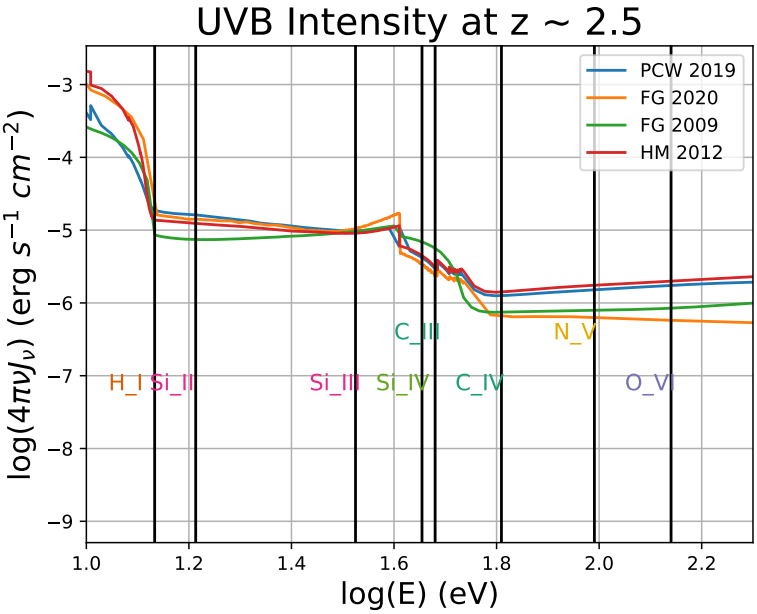

Figure 2: Indicates the energy distribution of two of the newest UVB models at redshift 2.5, FG 2020 and PCW 2019. The x-axis is the energy of the UVB in units of eV and the y-axis is the intensity of the UVB in units of $ergs^{-1}cm^{-2}$. Elias is working to get the older UVBs on this plot. The table format is... interesting.. Got them all plotted. Offset of HM 2012 is definitely wrong as I could not figure out correct unit conversions. [BWO: Need to tighten up the y-axis and make lines thicker, text larger so it's easy to see. I think we also ought to make a data table with all of this information and make it publicly available – people will really appreciate it and refer to the paper!]

Moving to the other end of our pipeline, we use trident to mimic physical observations by generating a series of randomly oriented lines of sight, or "rays" through the CGM. In this way, we generate 100 rays through our simulated galaxies. SALSA and Trident work together on this. SALSA calculates random start and end points for our rays given a central point, ray length, and a range of impact parameters. This lets us approximate observational sightlines passing within a certain distance (impact parameter) of the galaxy center. We'll need to report these geometric details. Trident is used to infer the ionic number densities using these CLOUDY-generated equilibrium ion fraction tables. Essentially, SALSA tells Trident what data to extract from the simulation. The important detail for our flowchart is that Trident "applies" the UVB to infer ionic number densities. [BWO: Make sure that Trident appears in the

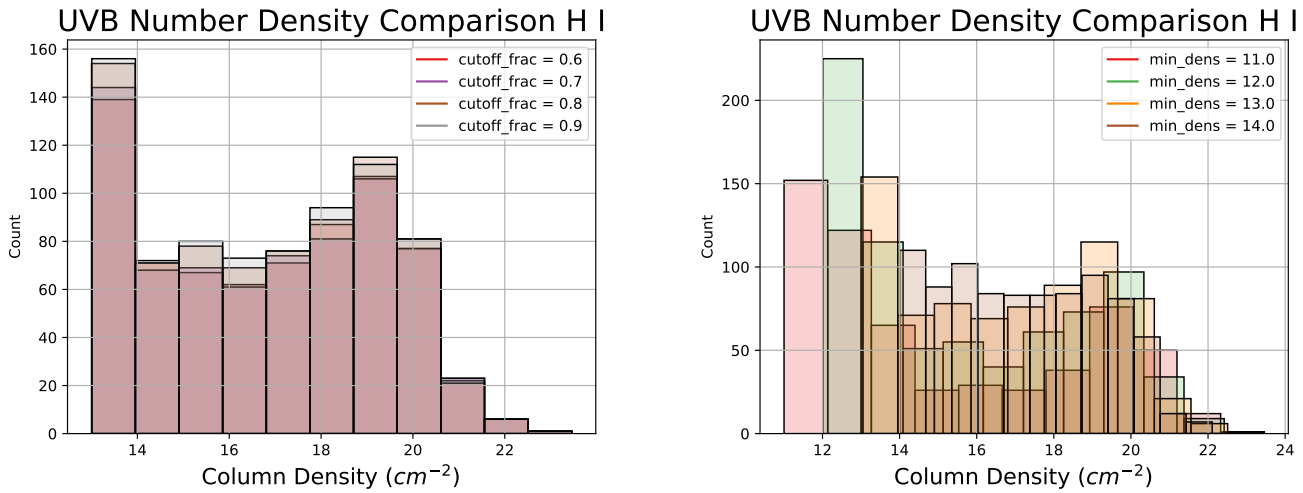

(a) (b)

Figure 3: a) A histogram showing the column density of SALSA absorbers produced at different cutoff fractions from 0.6-0.9 in intervals of 0.1. b) A histogram of SALSA absorbers produced at different minimum density thresholds from $log_{10}(11.0)$ to $log_{10}(15.0)$ in intervals of $log_{10}(1.0)$. Both figures: The x-axis is the number density in units of cm^{-3} and the y-axis is the fraction of the total data that exists at a given number density.

flowchart! Also, make sure to explain the maximum and minimum impact parameters as well as the virial radius of the halo(s) in question (we want to make it clear that we're actually looking at the CGM, not the ISM or IGM!).]

2.3. *Absorber Extraction*

Here, we take the rays generated by trident and iteratively identify absorbers along the line of sight for each ion using the Simple Procedure for Iterative Cloud Extraction (SPICE) method. This code works by setting a threshold above which some chosen percent (by default this is at 80% (**?**)) of the total column density along the ray is contained. Then, using this cutoff, bounds are set that define distinct "clumps" of gas that now appear within the data. That is, "clumps" are identified that account for 80% of the total column density of the line. On the next pass, additional regions are flagged that account for 80% of the column density that remains unaccounted for after the first pass. Clumps from each pass are combined by. This process is repeated until the column density of the remaining data that has not been assigned to an absorber is below the minimum density threshold ((the default for this is at 10^{-13} particles per cm^{-2} (**?**))). Then the velocity dispersion of each of the absrobers are compared with one another. If their dispersion is within a certain range (default is 10 km/s), they are considered to be the same absorber, otherwise they are labeled as two separate absorbers.

2.3.1. *Selecting SALSA Parameters*

In most of its use case, the percentage of total column density and minimum column density threshold are set to their default settings (80% and 10^{-13} respectively). Both of which are set arbitrarily. Therefore, to ensure the efficacy of our results, we employ a pseudo-grid search to determine the optimal set of parameters to apply to this algorithm. We define this pseudo-grid search as analysing the observed changes in $\log(N_{HI})$ found by independently varying both parameters (the parameter not being analyzed is left at its default setting). It should be noted that we did not investigate the non-linear effects from varying both settings at once.

From our variation of the cutoff fraction in fig. 3 (a), we find that the overall distribution remains consistent throughout the different settings used, but the total number of absorbers that SALSA identifies steadily decreases with increasing cutoff fraction. In fig. 3 (b), we see the same trend a with the cutoff fraction plot in which increasing minimum density results in fewer absorbers detected in addition to the distribution of column densities shifting towards higher densities.

2.4. *Absorber Categorization*

The UVB will affect the ionic number densities of the ray and therefore the clumps identified by the iterative SPICE algorithm. Once the SPICE algorithm has been run, we choose to perform our analysis via a pairwise comparison in which we take corresponding absorbers from two different UVBs and categorize them into different groups based on their relative position/size to one another along a given ray. The categories are as follows:

1. Match: absorbers are of the exact same size (meaning they cover the same number of simulation cells and spatial position along the ray
2. Different Size: the two absorbers are different sizes, but match in either start or end position. One UVB results in a clump that is longer or shorter than another UVB, but they still occupy the same physical region along the ray.
3. Overlap: absorbers have a significant overlap with one another along the line of sight, but they do not line up in terms of size or position (i.e. they do not share a start or end point and may encompass a differing number of cells.
4. Merge: when one of the UVBs contain multiple small absorbers, the other UVB contains only one large absorber
5. Lonely: there exists an absorber in one UVB while the other UVB has no absorber

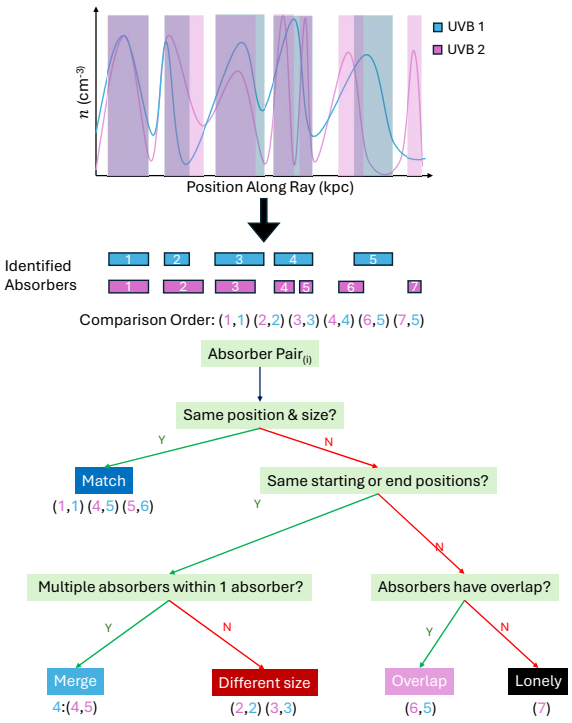

Figure 4: Diagram showing a flow chart of how the pairwise comparison algorithm. Each absorber is numerically labled in the order they appear along the ray. The "comparison order" list indicates the order in which pairs of absorbers are put through the flow chart. We might replace this with a sketch that highlights all 5 category types.

All of these comparisons are made using a series of boolean logic with some margin of error allotted. Selecting the exact margin of error for this analysis is quite difficult as the ray is indexed by dl, the length of the ray passing through

Ion	FG 2009	FG 2020	HM 2012	PCW 2009	FG 2020	PCW 2019
H I	0.05	0.01	0.02	0.0	0.01	0.01
Si II	0.02	0.01	0.01	0.01	0.10	0.01
Si III	0.01	0.05	0.0	0.31	0.14	0.04
C III	0.01	0.03	0.01	0.03	0.01	0.03
Si IV	0.01	0.05	0.01	0.04	0.15	0.03
C IV	0.01	0.02	0.01	0.05	0.08	0.02
N V	0.03	0.1	0.04	0.03	0.09	0.19
O VI	0.05	0.05	0.03	0.04	0.08	0.11

Table 1: Pairwise comparison between UVBs showing the fraction of absorbers categorized as lonely by the absorber categorization algorithm for each ion

Ion	FG 2009 & FG 2020	HM 2012 & PCW 2019	PCW 2019 & FG 2020
H I	0.05	0.02	0.02
Si II	0.0	0.04	0.01
Si III	0.02	0.03	0.04
C III	0.02	0.04	0.06
Si IV	0.02	0.01	0.01
C IV	0.05	0.03	0.05
N V	0.0	0.03	0.01
O VI	0.0	0.09	0.15

Table 2: Pairwise comparison between UVBs showing the fraction of rays that were removed due to the absorber sorting algorithm being unable to categorize them

the in-simulation cell. Since the orientation of the ray is random, the physical size of each index along the ray as the *dl* quantity will not be consistent between indices. This will also vary between each ray as each ray will be created in a unique orientation. To address this issue, we have decided to adjust the margin of error, such that it has the lowest number of "outlier matches", absorber pairs that are categorized as matches while existing outside the general trend of the match data. This hinges on the assumption that absorbers that share similar spatial coordinates have similar physical quantities (gas density and temperature). Using this method, we found that 7 in-simulation cells was the optimal margin of error.

Once these comparisons are completed, we then begin the process of condensing the data to allow for more accurate comparisons between the UVBs. The merger cases were condensed so that the smaller absorbers in the set were combined to match the larger absorber. As for the other physical quantities of the absorber such as tempurature, gas density, and metalicity were combined by weighted average based on the column densities of the individual absorbers by the following equation:

$$\frac{x \cdot \sigma}{\sum_{i=1}^{n} \sigma_i}$$

Where n is the number of absorbers within the set undergoing combination, x is the array of a given physical quantities of length n, and σ is the array column densities also of length n. Note that SALSA already reports a column density-weighted average of these quantities. For merged clumps, we further combined them using weighted averaging.

Lonely cases were removed from the analysis due to their rarity along with the fact that displaying such data hid some of the more interesting results of our analysis.

Additionally, there were a few rays in which the sorting algorithm was unable to determine which category in certain sets of absorbers fell into. These cases entirely consisted of absorbers that fell into multiple categories. Instead of handling all of these outliers, the rays are removed from the analysis. The fraction of removed rays are as follows:

3. RESULTS

We now present a series of figures comparing the column density between each UVB model along with several other physical quantities such as gas density and temperature. However, before showing these comparisons, we first compare

the total column density of each ray as generated by trident. This acts as a sanity check for our SALSA results to ensure the column densities we see are accurate. This is shown in fig 5. Here, we find that the total column density remains fairly consistent between the generational comparisons (that is, UVB model comparisons between models from the same authors) while the comparison between model families (FG 2020 and PCW 2019) show significant differences between one another. The only ions we see some similarity is in Si II, Si IV. We also find that ions in higher ionization states tend to results in larger differences for these comparisons. H Iappears to be an exception from this trend with comparisons HM 2012 / PCW 2019 and FG 2009 / FG 2020 both having a distinct dip at 10^{22} cm^{-2}. This shows that the column density of PCW 2019 and FG 2020 have significantly higher densities of H Ithan in other UVB models. expanding the analysis to include comparisons FG 2020 with HM 2012 and PCW 2019 with FG 2009, we see very similar "dips" at the same column density. This, along with the very strong agreement between the more recent models, indicates that the differences we see are likely due to the updated observational data in the newer models.

With this context in mind, we now discuss the results of the SALSA algorithm for each of these comparisons

3.1. *Figure 6: FG09 vs FG20*

For our first comparison, fig. 6, our results appear to be mostly within expectation. For H I, we see that FG 2020 has systematically lower column densities of H I than FG 2020, which appears to peak at a specific gas density of 0.1 cm^{-3}. This peak also seems to correspond with a temperature of around $10^{4.2}$ K. While there are some outliers where FG 2020 has much higher density than FG 2009, these absorbers fall into the overlap category, where the spatial positioning between the two absorbers does not match very well. Si IIappears to have match very well between the two UVB models with the largest differences appearing to be in favor of FG 2009 in the same "peak" pattern that we see in H I. In Si III, there are systematically higher densities of in FG 2020 with a very strong parabolic trend with gas density an no noticable trends with temperature. C IIIand Si IVseem to follow very similar trends with the main difference between the three ions being on the gas density plot that the right-tail-end of the parabolic structure tends to flatten with increasing ionization energy. In C IV, we see FG 2020 systematically slightly higher column density. As column density and overall gas density increase, the agreement between the two UVBs tends to increases. This is very similar to the previous three ions except there is noticeably more scattering and a more distinct trend with temperature with less model agreement at higher temperatures. N Vagrees very well between the tow UVBs, Though there is a noticeable spread in the data that forms as gas density increases and temperature decreases. O VIhas a very large spread with no noticable trends in gas density, but a slight downward trend as temperature increases. Overall, it appears as though the majority of outliers in the system tend to be from absorbers that are categorized as 'overlap' which does make sense given the larger spatial differences between the two absorbers.

3.2. *Figure 7: HM12 vs P19*

In the HM 2012 - PCW 2019 comparison, fig. 7, we find very similar results to the FG 2009 - FG 2020. In H I, we see the same pattern of a systematic larger density in the older UVB (HM 2012 in this case) followed by a large "bump" pattern around 0.1 cm^{-3} and $10^{4.2}$ K, Si IImatches fairly well between the two backgrounds. Si III, C III, and Si IVall also roughly follow the same parabolic pattern where higher density side of the parabola flattens with increasing ionization energy as seen in the previous comparison. C IValso appears to follow this trend, except there is now a more notable trend with PCW 2019 having larger absorber densities at higher temperatures. N Vappears to agree rather well, with PCW 2019 absorbers having higher column densities at lower gas densities, column densities, and higher temperatures. The O VI patterns appear to be much less scattered than the FG comparisons with trends very similar to those of the N Vin gas density. However, there are no significant trends with temperature.

3.3. *Fig 8: FG20 vs P19*

We now make our comparisons between model families. For H I, aside from a few outliers, we see that the two UVB models agree very well with one another in terms of their physical quantities, with low small error bars on the temperature and gas density plots along with a $\log_{10}$ column density ratio that is mostly centered around 0. For the rest of the ions, we see the same general pattern: At low column densities, gas densities and higher temperatures, FG 2020 has higher column densities, agreeing much more in high-density, low temperature regions. While we do see that the variance tends to increase with ionization energy, this trend appears to be the case for all ions outside of H I.

4. DISCUSSION

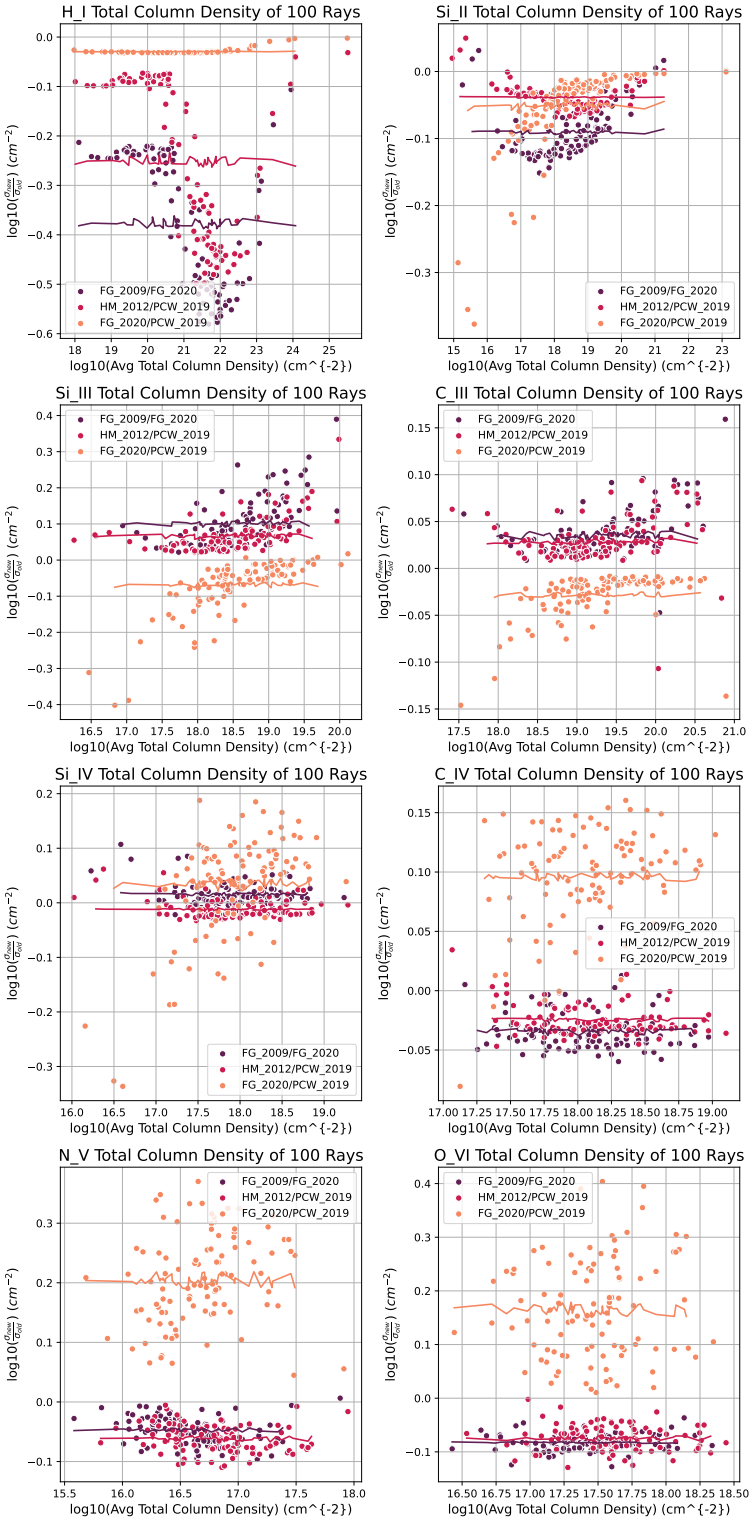

Figure 5: Each data point represents the total column density of a ray under a given UVB for a given ion. In the x-axis is the average column density between the two UVBs in the comparison, and the y-axis shows the log_{10} ratio between the older and newer UVBs.

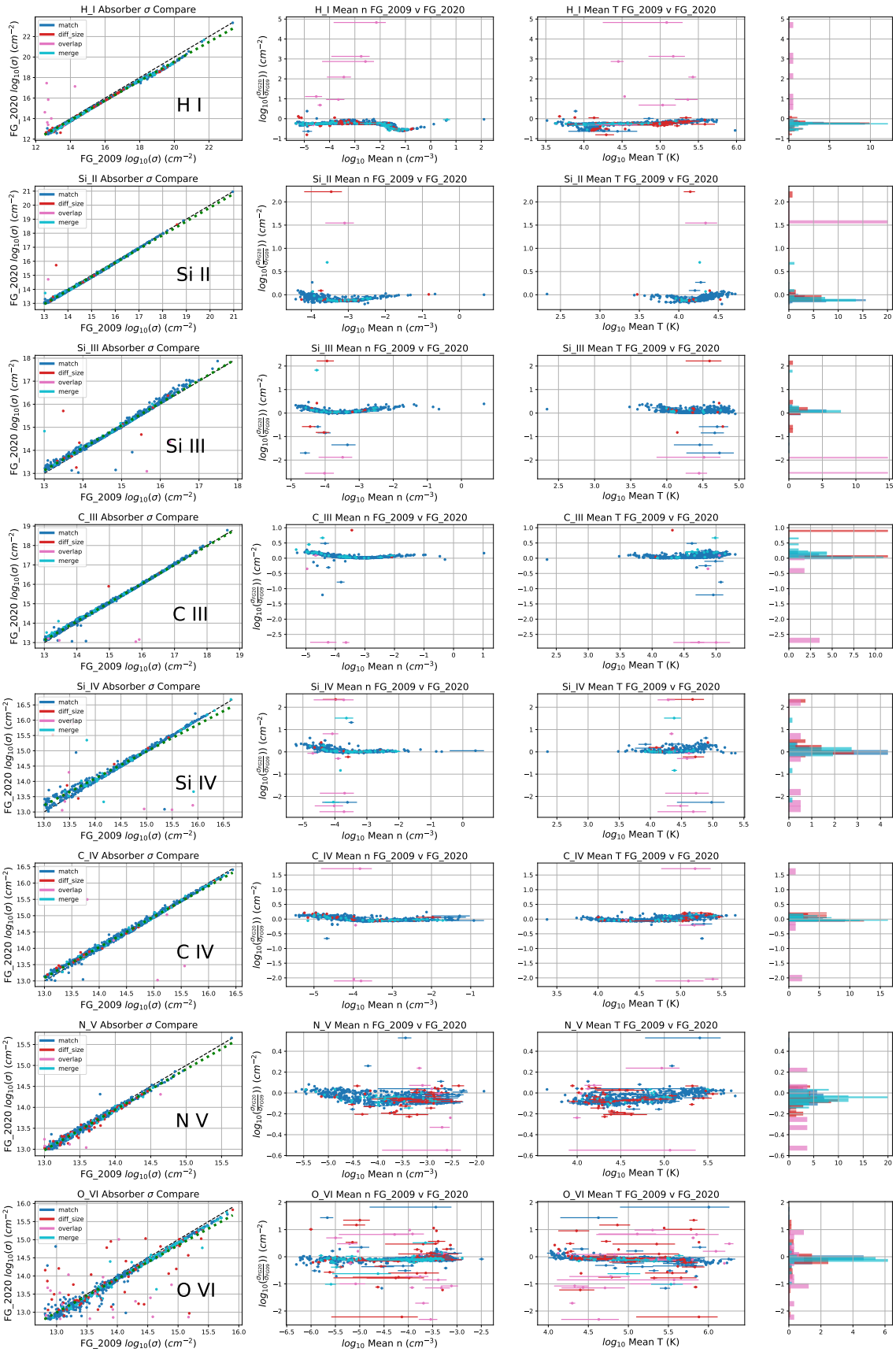

Figure 6: Compares the SALSA absorbers from the FG 2009 and FG 2020 UVB models based on their column density, temperature and gas density. The leftmost column is a direct comparison between column densities with FG 2009 column densities in the x-axis and FG 2020 in the y-axis. A dashed black line is included to represent the "match" line where the two absorber column densities match with one another. Additionally, a green dotted line is included as a linear fit generated to the comparison scatter. In the next column to the right is the gas density comparison where the x-axis is the average gas density (n) between the two UVB models with errorbars showing the lower and higher

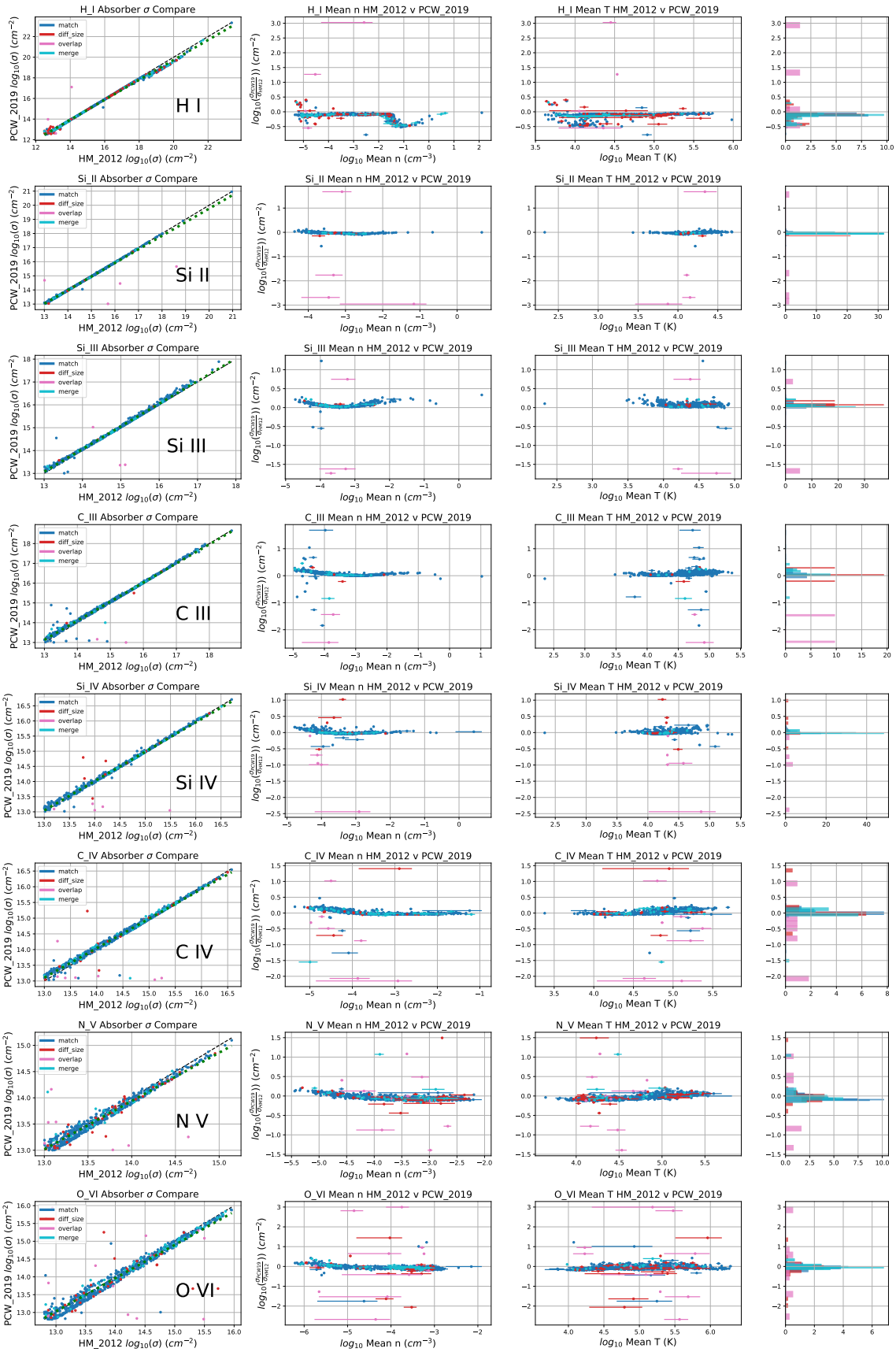
H_I Absorber σ Compare
H_I Mean n HM_2012 v PCW_2019
H_I Mean T HM_2012 v PCW_2019
Si_II Absorber σ Compare
Si_II Mean n HM_2012 v PCW_2019
Si_II Mean T HM_2012 v PCW_2019
Si_III Absorber σ Compare
Si_III Mean n HM_2012 v PCW_2019
Si_III Mean T HM_2012 v PCW_2019
C_III Absorber σ Compare
C_III Mean n HM_2012 v PCW_2019
C_III Mean T HM_2012 v PCW_2019
Si_IV Absorber σ Compare
Si_IV Mean n HM_2012 v PCW_2019
Si_IV Mean T HM_2012 v PCW_2019
C_IV Absorber σ Compare
C_IV Mean n HM_2012 v PCW_2019
C_IV Mean T HM_2012 v PCW_2019
N_V Absorber σ Compare
N_V Mean n HM_2012 v PCW_2019
N_V Mean T HM_2012 v PCW_2019
O_VI Absorber σ Compare
O_VI Mean n HM_2012 v PCW_2019
O_VI Mean T HM_2012 v PCW_2019
match
diff_size
overlap
merge
H I
Si II
Si III
C III
Si IV
C IV
N V
O VI
PCW_2019 log10(σ) (cm−2)
HM_2012 log10(σ) (cm−2)
log10 Mean n (cm−3)
log10 Mean T (K)

Figure 7

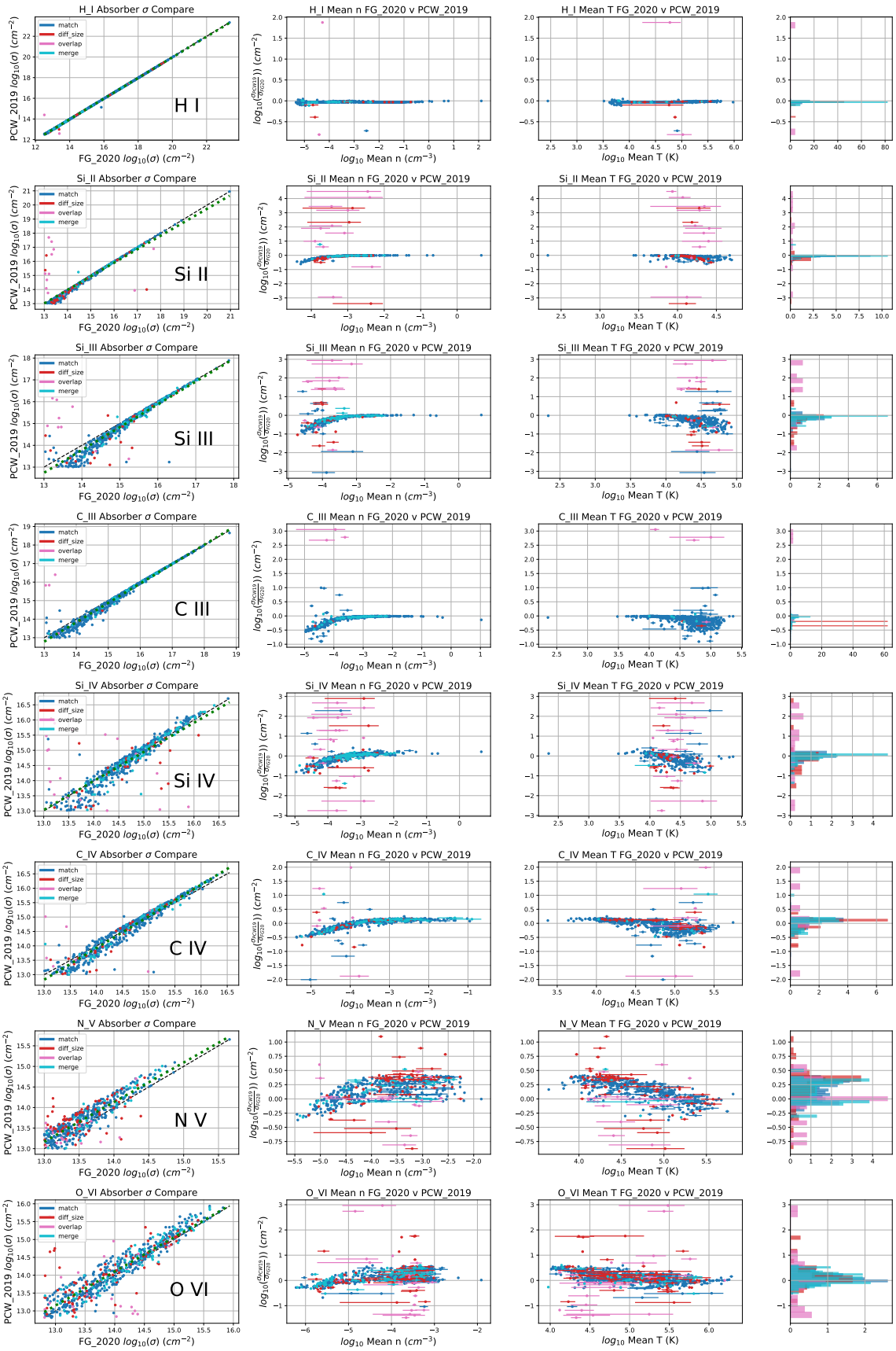
H_I Absorber σ Compare
H_I Mean n FG_2020 v PCW_2019
H_I Mean T FG_2020 v PCW_2019
Si_II Absorber σ Compare
Si_II Mean n FG_2020 v PCW_2019
Si_II Mean T FG_2020 v PCW_2019
Si_III Absorber σ Compare
Si_III Mean n FG_2020 v PCW_2019
Si_III Mean T FG_2020 v PCW_2019
C_III Absorber σ Compare
C_III Mean n FG_2020 v PCW_2019
C_III Mean T FG_2020 v PCW_2019
Si_IV Absorber σ Compare
Si_IV Mean n FG_2020 v PCW_2019
Si_IV Mean T FG_2020 v PCW_2019
C_IV Absorber σ Compare
C_IV Mean n FG_2020 v PCW_2019
C_IV Mean T FG_2020 v PCW_2019
N_V Absorber σ Compare
N_V Mean n FG_2020 v PCW_2019
N_V Mean T FG_2020 v PCW_2019
O_VI Absorber σ Compare
O_VI Mean n FG_2020 v PCW_2019
O_VI Mean T FG_2020 v PCW_2019
match
diff_size
overlap
merge
H I
Si II
Si III
C III
Si IV
C IV
N V
O VI
PCW_2019 log10(σ) (cm−2)
FG_2020 log10(σ) (cm−2)
log10 Mean n (cm−3)
log10 Mean T (K)

Figure 8

For our initial total column density comparison in fig. 5, we find that the data appears to be in agreement with fig. 2. This is especially evident with H Iwhere in fig. 2, we see a distinct difference between the newer and older generations' intensity at 1 Rydberg, where the newer generations model have higher intensities than the older models, and as we might expect, we see that in fig. 5, the older models have systematically higher densities. However, this does not explain the distinct dip around 10^{19} cm^{-2}. This is (I don't actually know why this exists). Unfortunately, we cannot extend this logic to the rest of the ions in the figure as the relationship between the UVB spectra and ion abundances becomes much more complex with species that have higher and lower ionization states.

For the SALSA-processed, absorber-categorized data (fig 6-8), we find that our results are physically viable. The column density ratio scattering tends to increase with increasing ionization energy, which makes sense as ions with larger ionization energies are more difficult to predict with photoionization as collisional ionization begins to dominate. We also find that the vast majority of absorber pairs were classified as "match" and tend to agree very well between the two models being compared in terms of column density, gas density and temperature. Gas density tends to have a very strong relationship with column density. This is because the gas density is an integral of the column density. While SALSA does complicate this process, we are using the same algorithm across all samples, so this complication is mitigated somewhat. Temperature has noticeably weaker trends with column density, however we still see that the majority of differences occur in regions of higher temperatures while lower temperature regions tend to have more agreement between models. In summary, we see the largest differences between models in regions of higher temperature and lower density, where photoionization, and thereby the UVBs, have the most impact on ionization.

There is a very strong distinction between comparisons within model families and comparisons between model families. This is most clear in the H Icomparisons in which in fig 6 and fig. 7 have a distinct "dip" that does not exist in fig. 8.

In the case of PCW 2019, this is due to new photoionization and photoheating rates as well as new calibrations to reach a higher optical depth ($\tau_e = 0.065$) to match the Plank 2015 observations (Faucher-Giguere, 2020). For FG 2020, they make a number of updates based on: updated galaxy UV luminosity functions, a new stellar spectral template, new AGN luminosity functions, improved IGM opacity measurements, (Faucher-Giguere, 2020)

Though it is important to note that the FG 2009 - FG 2020 comparison has a larger scatter than that of the HM 2012 - PCW 2019 comparison. This is because while PCW 2019 only changes the fitting parameters based off new observational data, FG 2020 includes binary stars in its analysis.

It should also be noted that in addition to σ and n we also tested metalicity (Z) to see if we could find any relationships with the absorber column density ratios, however, we did not find any correlation between any of the ions we tested.

- how does knowledge about the changes in model generations help explain trends (both from whatever new insights encouraged the updated in the first place and from looking at the ionization fractions themselves

4.2. *Comparison to Other Literature*

As of late, works such as our own, focused on characterizing the uncertainties produced by the UVB have become a topic of much discussion as of late. The vast majority of which, focus on reverse modeling approaches to understand its complexities. One such work is from Gibson et al. 2022, a study focusing that contributes to this discussion as well. This study focuses on allowing the power-law slope of the UVB vary as a free parameter. Doing so causes uncertainties in CGM ion column densities to increase from 0.08 to 1.14 dex.

In comparison to other works looking to investigate uncertainties introduced by UVB models, Mallik et al. 2023 investigates a very similar topic to the one addressed within this work. In this paper, Mallik et al. 2023 performs both a forward and backward modeling approach, looking at the impact of UVB on simulated absorption features and their subsequently inferred column densities rather than directly looking at the absorbers themselves. Although this leads to more sources of uncertainty, it also produces results that are much more comparable to observation. Our work helps expand upon the findings of Mallik et al. 2023, showing that the uncertainty in metal absorbers exists not only through the forward-backward modeling approach taken in their paper, but within the distribution of absorbers themselves. Another work, Acharya and Khaire 2022, also finds similar results in their study. This work also employs reverse modeling techniques via the creation of "toy" absorbers, using CLOUDY to recover the H Inumber density and metallicity. Here, they find very similar results to our work, with the main differences being the authors only used H Iin their analysis and had a much more significant focus on inferred physical quantities as opposed to inferred column density. Regardless, our work also serves to extend the results of this paper, showing the variance between the

different UVB models result in differences for multiple ion species in both forward modeling and backward modeling approaches. In opposition of these backward modeling approaches, Marra et al. 2024 finds that there is some caution to be had with this methodology and the assumption that all of the absorption features of a cloud originate from a singular absorber. In their work, they found that a significant portion of the features of absorption spectra appear from sets of multiple absorbers, a significant portion of which do not share common gas mass. This serves to support our forward modeling approach as we are completely able to avoid introducing the uncertainty from this assumption into our analysis.

Another study that analyzes the CGM at $z \approx 2$, Lehner et al. 2022 analyzes the metalicity of CGM absorbers observed by KODIAQ-Z as compared to FOGGIE simulation data. To extract absorbers from the FOGGIE galaxies, the authors also use SALSA, using HM 2012 as the UV background for their analysis. Given the insights of our work the metalicity in their analysis would likely remain relatively unchanged, regardless of which UVB model was used. However, there would likely be some changes in the H Icolumn densities around $10^{18} - 10^{20}$ cm^{-2} range as more recent models have significantly lower gas densities of H I$(\approx 0.5dex) in this column density range.$

4.3. *Limitations*

One drawback of this work stems from our direct analysis of absorbers that are physically contiguous, extracting their column densities rather than estimating the column density via absorption spectra. While our approach may not be the most conventional, the goal of this work is ultimately to compare impact of different UVB models, and the most direct way to understand the physical impacts is by looking at the absorbers themselves. In this way, we avoid any additional variables that may confuse the results of the analysis.

Additionally, the variables used in the iterative process of SALSA, cutoff fraction and minimum density are still arbitrarily selected, despite our efforts to calibrate them. Future work may consider calibrating these quantities against observational data to further increase accuracy. There is also the use of boolean logic in the absorber categorization script in which the margins of error for establishing these categories are set arbitrarily. This is further complicated by the random physical sizes of each cell along the randomly oriented ray objects (see sec 2) which lowers the accuracy of setting a single error margin based around ray cells as each ray cell is not the same size, nor are they the same size between different rays. Future studies should attempt to remedy these issues by instead setting an error region based around physical size rather than cell indices. Finally, our work has some inconsistencies as we are using temperature, density, metallicity values that come from using a specific UVB in the FOGGIE simulations (which one was it?), then post-processing them with different UV backgrounds. Unfortunately, this is the only way to perform absorber-by-absorber matching as rerunning entire simulations under different UVBs is far to computationally expensive to be feasible within the bounds of this project.

5. CONCLUSIONS

In this paper we have utilized CLOUDY to generate ionization tables from more recent UVB models, performed a psuedo-grid search to optimize the SALSA absorber extractor algorithm, generated 100 randomly-oriented rays through a simulated FOGGIE galaxy, utilized SALSA to extract absorbers from each ray under four different UVBs: FG 2009, FG 2020, HM 2012 and PCW 2019, ran an absorber-categorization algoithm to perform a pairwise sort through respective SALSA absorbers to categorize them and remove absorbers that could not be compared. Finally, we analyzed our results via a series of plots comparing the column density differences with gas density and temperature.

From our analysis, we found:

1. Observed column densities show significant differences between UVBs, with notable patterns between model generations and between model families

2. the differences between UVB are most significant in regions where they are the most effective (low density, high temperature)

3. our work agrees with much of the current literature that focused on backward modeling

There are several areas of uncertainty in this work that may be pursued in future works. Firstly, concerning variation in elemental abundances. We assume in this work that all gas, regardless of metallicity, has the Solar abundance ratios (this is also an assumption that is typically made when analyzing actual observational data). This is not always true, and in fact we would expect that the (non-hydrogen) elements that are commonly observed in the CGM would

have some variation in their relative abundance – carbon comes from both massive stars and low-mass stars, whereas oxygen and magnesium come entirely from massive stars, and even the elements that come from the same sources don't necessary end up with precisely the same ratios. This is an obvious point of future work. We also must consider the inclusion of the variation of the UV background near galaxies due to the massive stars in that galaxy. This is potentially important at low impact parameters (i.e., close to the galaxy itself), and it likely also depend on the azimuthal angle – i.e., UV light from stars is going to be preferentially escape along the poles rather than in the equatorial plane. Again, an area for future work. Lastly, the velocity blending of absorbers (getting one step closer to actual observations). This is justifiable because we have constrained our analysis in a specific way, but if we were trying to get closer to observations this would be an important factor.

6. QUESTIONS FOR MOLLY AND JASON

- Given the wide variety of ions and limited amount of figures we can include, what are some of the ions we can include that would be most useful to observers? Figure 5 might be helpful here.
- Are the column densities SALSA is determining consistent with what we might expect from the FOGGIE simulations?
- Are there any other ways of presenting our data that might make our comparison between these different UVBs more effective?
- the SALSA code takes in a few parameters that were initially determined arbitrarily as seen in section 2.3.1. While the cutoff fraction parameter doesn't result in significant changes in SALSA gas density distributions, the minimum density parameter appears to cause significant changes in our results, and we're unsure as to how we want to handle this issue. Setting a lower minimum density threshold allows for more low column density clumps (as one might expect). It is possible to set a different threshold per ion. What's reasonable here?
- what other statistical measures might be useful to help quantify the trends seen by eye?

Facilities: HST(STIS), Swift(XRT and UVOT), AAVSO, CTIO:1.3m, CTIO:1.5m,CXO

Software: astropy (Astropy Collaboration et al. 2013, 2018), Cloudy (Ferland et al. 2013), Source Extractor (Bertin & Arnouts 1996)

APPENDIX

A. APPENDIX INFORMATION

B. AUTHOR PUBLICATION CHARGES

REFERENCES

Astropy Collaboration, Robitaille, T. P., Tollerud, E. J., et al. 2013, A&A, 558, A33, doi: 10.1051/0004-6361/201322068

Astropy Collaboration, Price-Whelan, A. M., Sipőcz, B. M., et al. 2018, AJ, 156, 123, doi: 10.3847/1538-3881/aabc4f

Bertin, E., & Arnouts, S. 1996, A&AS, 117, 393, doi: 10.1051/aas:1996164

Ferland, G. J., Porter, R. L., van Hoof, P. A. M., et al. 2013, RMxAA, 49, 137. https://arxiv.org/abs/1302.4485